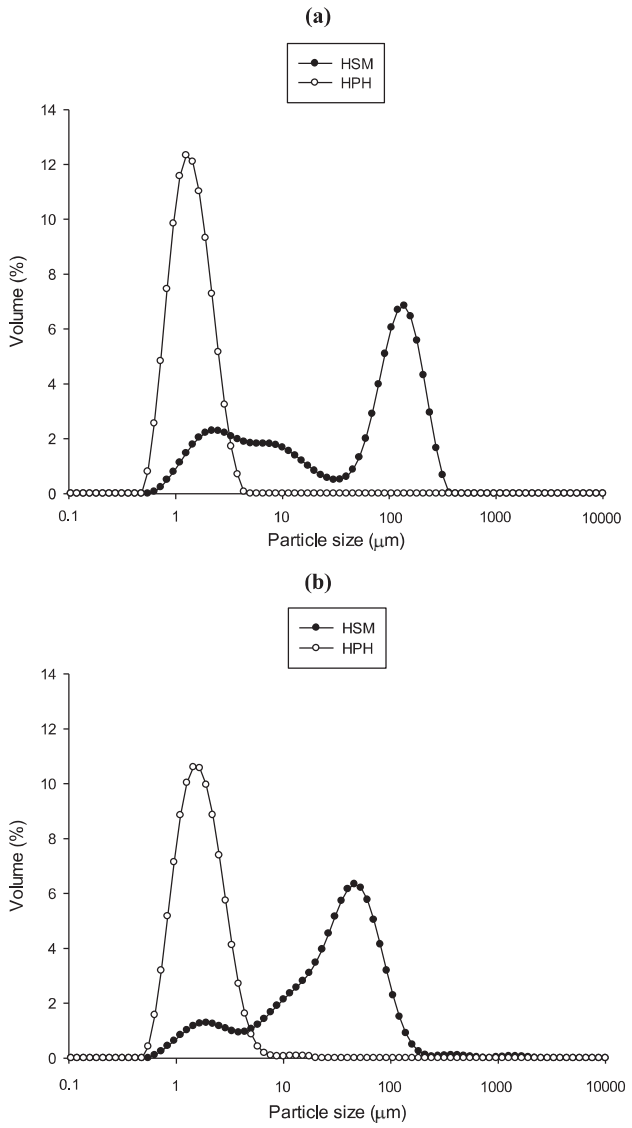

Figure 8. Droplet size distribution of the O/W Pickering emulsions stabilized by CNCs (a) and CNFs (b) homogenized by HSM (—●—) or HPH treatment (—○—).

stand the impact of the morphological properties of NCs on the viscosity of the emulsions and its relation to stability, rheological properties of the emulsions were evaluated. The Pickering emulsions stabilized by CNCs and CNFs exhibited typical shear-thinning behavior, wherein the apparent viscosity decreased with increasing shear rate. Specifically, for CNFs, this behavior was observed across the entire shear rate range of 0.1 to 100 s^{-1}, while for CNCs, a plateau was reached at shear rates higher than 1 s^{-1}. This behavior is linked to the structural deformation of the emulsion, with the breakdown of entangled 3D networks and orientation along flow lines occurring more easily for CNCs emulsions (**Figure 10**).[60,61] Moreover, CNFs contributed to increased emulsion apparent viscosity values[62] compared to an equivalent amount (mg mL^{-1}) of CNCs, likely due to their greater flexibility and defibrillation, allowing the formation of internal entanglements in the continuous phase. These entanglements, combined with the Van der Waals- or hydrogen bond-mediated fiber-to-fiber interactions, restrict the movement of the oil droplets and enhance emulsion stability.

Table 2. Particle size distribution (expressed as characteristic diameters and span) of Pickering emulsions homogenized by HSM or HPH treatment and stabilized by CNCs and CNFs.

	O/W Pickering emulsion stabilized by CNCs		O/W Pickering emulsion stabilized by CNFs	
	HSM	HPH	HSM	HPH
d(0.1) [μm]	2	1	3	1
d(0.5) [μm]	70	1	30	2
d(0.9) [μm]	180	2	79	3
D[4,3] [μm]	77	1	42	2
D[3,2] [μm]	6	1	8	1
Span (−)	3	1	3	1

2.3. Stability of NCs-Stabilized Pickering Emulsions

Emulsifying activity and emulsion stability, evaluated through EAI and ESI values, respectively, are recognized as crucial parameters for assessing the emulsifier's efficacy in forming a stable emulsion. EAI and ESI values, presented in **Table 3**, are greatly influenced by the hydrophobicity and ionic charge of CNCs and CNFs. A significantly ($p < 0.05$) higher value of interfacial area stabilized per unit of weight (EAI = 186 ± 4 m^2 g^{-1}) was observed for CNCs compared to CNFs, likely attributed to the smaller molecules of CNCs, facilitating quicker diffusion and adsorption onto the oil–water interface.[63,64]

This behavior can be explained in terms of the observed differences in interfacial tension (14 and 19 mN m^{-1} for CNFs CNCs, respectively, at 2000 s), which are expected to influence emulsifying performance. This includes their ability to interact with the oil–water interface and facilitate droplet formation, while the high surface charge density enhances droplet stability through electrostatic repulsion.[56]

Simultaneously, ESI was found to be 0.14 ± 0.03% and 0.33 ± 0.09% for CNCs and CNFs-stabilized emulsions, respectively. The higher ESI observed for CNFs-stabilized emulsion significantly differed ($p < 0.05$) from that stabilized with CNCs, likely due to the greater molecular flexibility of CNFs, a crucial factor in forming a compact interfacial layer and promoting emulsion stability.

Remarkably, the results in Table 3 show that the effect of HPH was more pronounced for CNFs-stabilized emulsions than for CNCs-stabilized ones: EAI values increased tenfold for the former and only doubled for the latter upon HPH processing, aligning with the morphological data discussed earlier. Therefore, thanks to HPH treatment, the emulsification ability (EAI) of CNFs becomes comparable to that of CNCs. The capability to stabilize emulsions (ESI) was higher in CNFs-stabilized emulsions, primarily due to the higher viscosity of the continuous phase, which slowed down gravitational separation phenomena.

To assess the long-term stability of various types of NCs in Pickering emulsions, changes in microstructure and mean droplet diameter were monitored over a 10-month period at 5 °C.

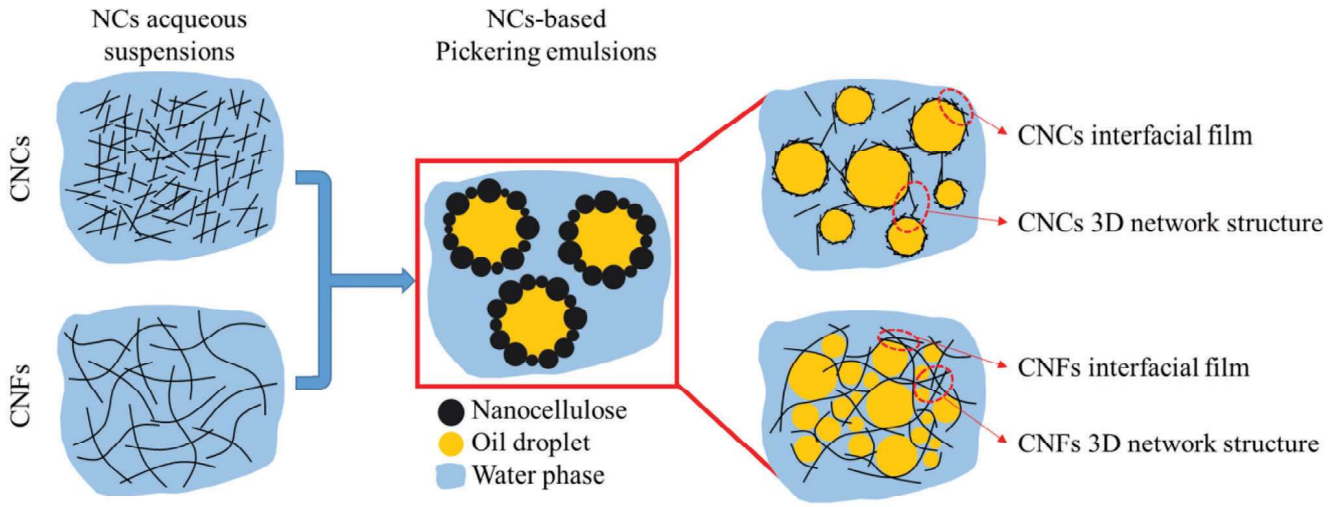

Figure 9. Schematic illustration of stabilization mechanisms of CNCs- and CNFs-based Pickering emulsions.

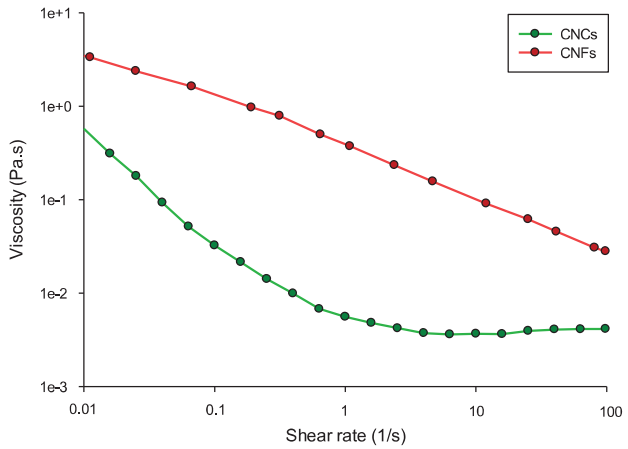

Figure 10. Rheological properties of emulsions prepared by HPH and stabilized by CNCs (—●—) and CNFs (—●—).

Figure 12 presents microscope images of emulsions stabilized by CNCs and CNFs. Visual observations show that CNCs efficiently stabilized Pickering emulsions, without exhibiting signs of precipitation or flocculation throughout the entire storage period.

Table 3. Emulsifying activity (EAI) and emulsion stability (ESI) parameters of Pickering emulsions homogenized by HSM or HPH treatment and stabilized by CNCs and CNFs.

	O/W Pickering emulsion stabilized by CNCs		O/W Pickering emulsion stabilized by CNFs	
	HSM	HPH	HSM	HPH
EAI [m^2 g^{-1}]	89.49 ± 6.60^b	186.03 ± 4.40^d	16.60 ± 1.54^a	150.02 ± 2.98^c
ESI [%]	0.05 ± 0.01^a	0.14 ± 0.03^a	0.15 ± 0.03^a	0.33 ± 0.09^b

Different letters denote significant differences ($p < 0.05$) among the different samples within each row ($n = 3$).

The appearance of CNCs-stabilized emulsion indicated no phase separation after 10 months.

Interestingly, after 10-month of storage, the mean droplet diameter of the emulsions decreased compared to the freshly prepared samples (Figure 12), indicating an unusual phenomenon, contrary to the coalescence of the particles, which could instead be expected during emulsion extended storage. This behavior can presumably be attributed to different mechanisms[65]: i) the strong electrostatic repulsion due to the high surface potential of the CNCs-coated oil droplets (ζ-potential of −46 mV (Table 1)); ii) the strong steric repulsion due to the rearrangement of CNCs layers around the droplets' surfaces, forming a network structure that effectively prevents oil droplets from coalescing into larger droplets during the emulsion aging process[66]; and iii) the irreversible adsorption of the CNCs at the oil droplet surfaces based on the Pickering stabilization.

In contrast, flocculation of the emulsions prepared with CNFs is evident at the end of the storage period, with the formation of aggregates visible to the naked eye and under optical microscopy (**Figure 11**). Generally, smaller particles stabilizing the water-oil interface require less energy for removal. In the present case, lower stability is associated with larger particles, possibly due to the bridging flocculation of CNFs, aligning with the observed increase in CNFs-based emulsion viscosity due to fiber entanglements in the continuous phase.

The formation of aggregates is also evident from the particle size distribution data in **Figure 12**, possibly arising from CNFs chain interactions leading to droplet flocculation through a particle bridging mechanism at water–oil interface. Moreover, the EAI and ESI values of the emulsions were determined after 10 months of storage. Emulsions, post-storage period, exhibited lower EAI values than those freshly prepared (54.27 ± 4.02 m^2 g^{-1} and 45.23 ± 4.16 m^2 g^{-1} for CNCs and CNFs, respectively), but constant ESI values (017 ± 0.10% and 0.32 ± 0.02% for CNCs and CNFs, respectively).

In addition to assessing the 10 months of storage, the influence of the external environmental stimuli, i.e., temperature, ionic strength, and pH on the physical stability of the Pickering

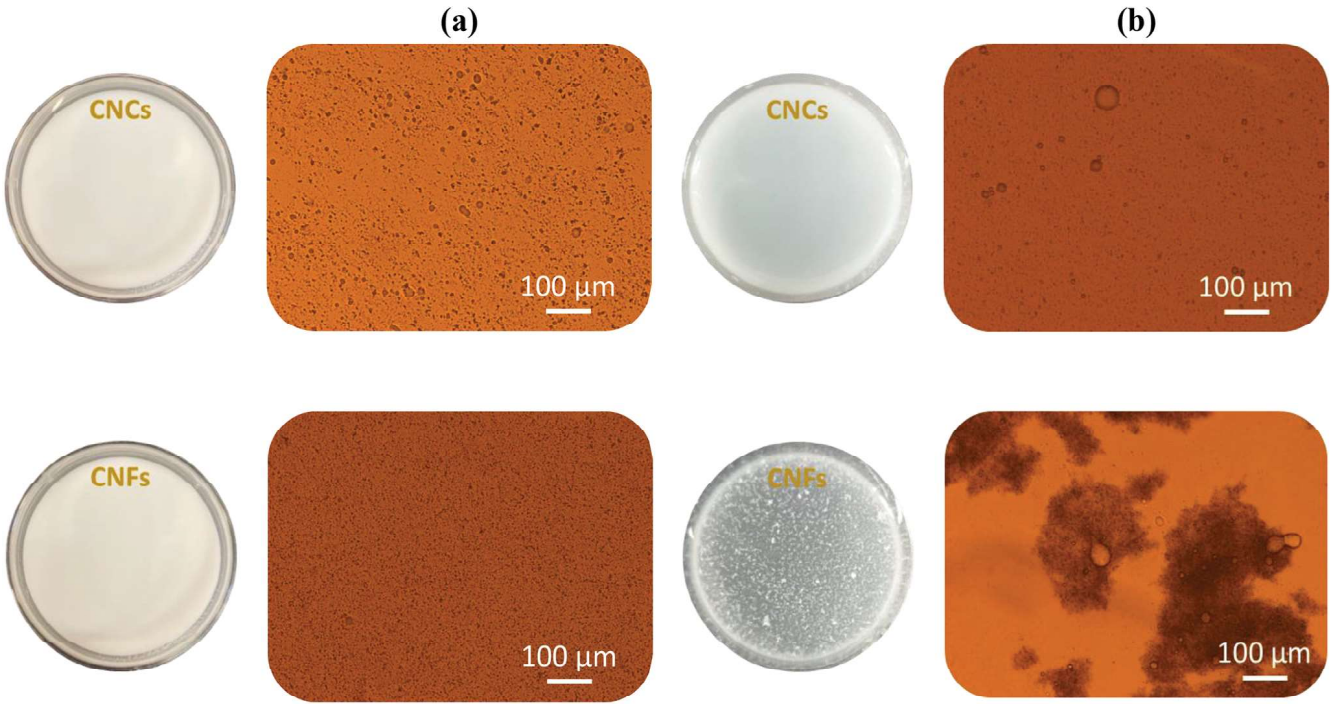

Figure 11. Visual observation and micrographs of (a) freshly prepared Pickering emulsions and (b) emulsions after 10-months of storage at 5 °C (10× of magnification) stabilized by CNCs and CNFs are presented in the first and second rows, respectively.

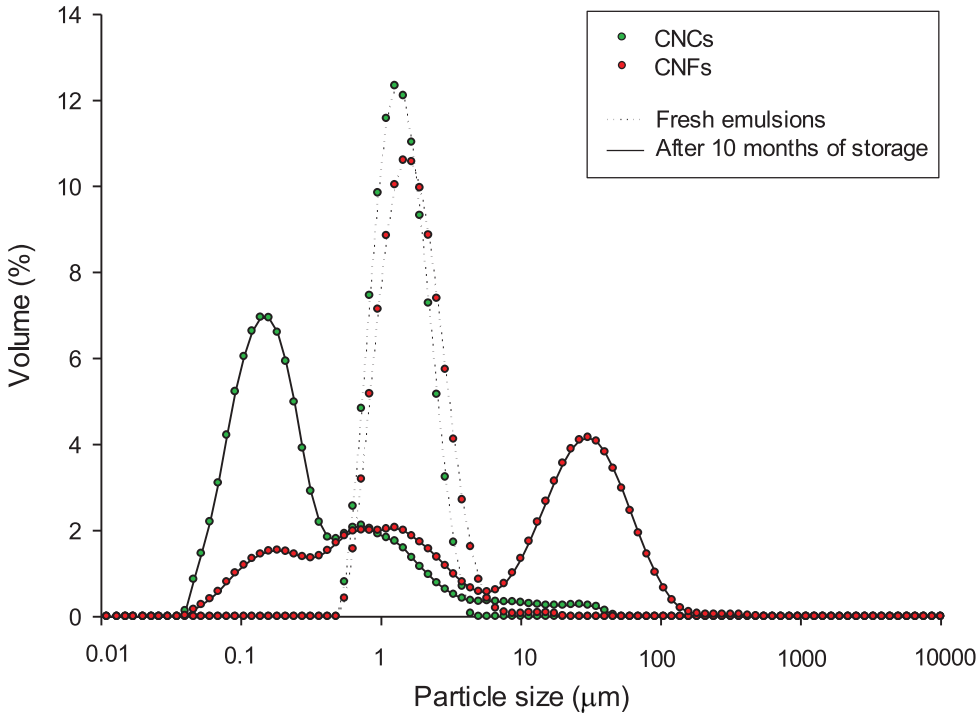

Figure 12. Droplet size distributions of CNCs and CNFs stabilized emulsions on day 0 (··· dotted line) and 10-months of storage (— solid line).

emulsion is of interest for application in in different fields. To this purpose, further studies are required for a comprehensive understanding of emulsion stabilization mechanisms.

The droplet size distribution measurements confirmed the microscopy observations, showing a decrease in droplet volume diameter for CNCs and an increase in CNFs after 10 months of storage (Figure 12). Remarkably, both CNCs- and CNFs-stabilized emulsions initially exhibited monomodal distributions, characterized by relatively small span values (1.17 and 1.40 for CNCs and CNFs, respectively) and transitioned to bimodal distributions during storage, with significantly larger span values (8.28 and 5.82 for CNCs and CNFs, respectively).

3. Conclusion

This study focuses on applying TEMPO-mediated oxidation to softwood kraft pulp Celeste 85 to obtain CNCs or CNFs, both possessing distinctive properties in terms of morphology, carboxylate group content, and wettability, are suitable for the stabilization of Pickering emulsions. These NCs are found to be suitable for stabilizing Pickering emulsions. The results show that the obtained CNCs, featuring a needle-like structure of ≈3 nm in thickness and ≈170 nm in length, and CNFs, characterized by a fibrous structure with dimensions of ≈10 nm in thickness and a few micrometers in length, effectively stabilize 5 wt% sunflower oil-based Pickering emulsions at a dosage of 0.5 wt%. Despite the significant morphological differences between CNCs and CNFs, both contribute to forming an interconnected network structure within the emulsion droplets, promoting efficient steric and electrostatic stabilization. Remarkably, when emulsions are produced via HPH, the treatment has a more pronounced effect on emulsification ability and stability on CNFs, likely attributed to a defibrillation process, enhancing CNFs performance to the level of CNCs. These results provide specific insights into how tailoring the properties of nanostructured cellulose during fabrication, through TEMPO-mediated oxidation and HPH, can be a straightforward strategy to influence the behavior and stability of Pickering emulsions. Specifically, CNCs can be employed in the stabilization of emulsions for low-viscosity applications, such as drinks and beverages, owing to the finer attainable emulsion size and span values. On the other hand, CNFs could find application in creams, sauces and dressings, benefiting from their higher apparent viscosity and the robust 3D-network formed by entangled fibers.

4. Experimental Section

Materials: Northern bleached softwood kraft pulp (Celeste 85) was a kind gift of SCA (Sundsvall, Sweden). This pulp was manufactured through a totally chlorine-free thermomechanical process and flush-dried.

Peanut oil, purchased from a local market (Olio di Semi di Arachide Giglio Oro, Firenze, Italy), was used as the oil phase in the experiment. According to the manufacturer's specifications, its composition on weight basis, comprises 18 wt% of saturated fatty acids, 46 wt% of monounsaturated fatty acids, and 28 wt% of polyunsaturated fatty acids.

Sodium dodecyl sulfate ($C_{12}H_{25}NaO_4S$, ACS GR, 99.0%, PanReac, Barcelona, Spain) was used as received without further purification. Milli-Q water (obtained with Barnstead Pacific TII Water, Thermo Scientific, Waltham, MA, USA) was used throughout the course of this study.

Preparation of NCs: TEMPO-mediated oxidation of cellulose pulp was conducted following the method of Saito and Isogai (Saito & Isogai, 2004), with slight modifications, as herein reported. To obtain CNCs, 5 g of Celeste 85 pulp were swollen in 400 mL H_2O. Subsequently, a solution containing 83 mg of 2,2,6,6-Tetramethylpiperidine-1oxyl (TEMPO, $C_9H_{19}N$, ≥98.0%, Alfa Aesar Chemicals, Ward Hill MA, USA), the reaction catalyst, and 0.5 g of sodium bromide (NaBr, ≥99.99%, Carlo Erba, Milan, Italy), the catalyst re-cycling, in 100 mL H_2O were added to the pulp suspension. The reaction was started by adding 18 mL of sodium hypochlorite containing 6–14% active chlorine (NaClO, Sigma–Aldrich, Milan, Italy), the primary oxidant. The pH of the reaction mixture was maintained within the interval 10.5–11 by incremental addition of NaOH until a constant pH was achieved, typically after 4 h. Subsequently, the suspension was rinsed several times with H_2O and was subjected to tip sonication at 80% power. The sonication process was carried out using a Bandelin Sonuplus ultrasonicator system (Berlin, Germany) on suspension aliquots of 35 mL volume. For the production of CNFs, the same procedure was employed, with the exception that a reduced quantity of TEMPO (12.5 mg) was used, and the reaction was terminated after 2 h.

Preparation of Pickering Emulsions: Coarse O/W emulsions were prepared by mixing peanut oil (5 wt%) with the aqueous phase (95 wt%) containing 0.5 wt% of CNCs or CNFs in ultrapure H_2O. The mixing process was carried out in a HSM (MIULab MT-30 K Handheld Homogenizer, Hangzhou, China) operating at 35 000 rpm for 5 min within an ice bath. Subsequently, the obtained coarse emulsions underwent further treatment through a HPH process at 80 MPa under recycle mode, for 15 equivalent passes, with the heat exchangers set at 5 °C. The HPH was performed using a laboratory setup, specifically an orifice-type homogenizer, as previously described in detail by Pirozzi et al.[42]

NCs Characterization: Atomic Force Microscopy (AFM) images were captured using an NT-MDT P47H probe microscope (Apeldoorn, Netherlands) scanning operated in the semi-contact mode with a tip spring constant of 40 N m^{-1}. Detailed information regarding the size and morphology of the CNCs and CNFs, produced by the TEMPO-mediated oxidation procedure, was obtained by analyzing these images with the Gwyddion 2.59 software.

Infrared spectra of CNCs and CNFs were acquired utilizing a Nicolet IN10 microFTIR instrument (Thermo Fisher Scientific, Waltham MA, USA) in transmittance mode. For this purpose, drops of CNCs' and CNFs' suspensions were deposited on ZnSe optical windows and left to dry in an oven.

The carboxylation of CNCs and CNFs was determined through conductometric titration using a Delta Ohm 2256 instrument (Padova, Italy). The samples were initially adjusted to pH 2.8 by the addition of HCl. Subsequently, the solution was titrated with 0.5 M NaOH. The degree of oxidation (OD), representing the carboxyl content per weight of CNCs and CNFs (μmol mg^{-1}), was calculated using Equation (1):

$$OD = \frac{C \cdot V}{m} \quad (1)$$

where C is the concentration of the NaOH solution, and m is the total mass of CNCs and CNFs measured after oven drying the suspensions. V is the volume of the NaOH solution added to reach complete ionization of COOH groups, which was obtained by fitting the experimental titration curve.[67]

The interfacial tensions of NCs (0.5 wt%) were determined through the pendant drop method using a contact-angle meter (KSV Instruments LTD CAM 200, Helsinki, Finland), equipped with an image analysis software. Briefly, a syringe equipped with a stainless-steel needle (0.71 mm in diameter) filled with the aqueous phase containing nanoparticles was submerged into the oil phase within a glass cuvette. Throughout the experiments, the initial volume of the formed drop was ≈30 μL. The contact angle meter recorded the dynamic change of the water–oil interface, and the Young–Laplace equation was subsequently used to calculate the interfacial tension. Distilled water was used as the control in these experiments. Interfacial tension (γ) measurements were performed over a pe-

riod of 2500 s, and equilibrium interfacial tension values were estimated using the exponential decay model of Equation (2)[68]:

$$\gamma = \gamma_\infty + (\gamma_0 - \gamma_\infty)\, e^{-\frac{t}{\tau_r}} \tag{2}$$

where γ_∞ is the asymptotic interfacial tension, γ_0 is the initial interfacial tension, τ_r is the characteristic time for the arrangement of the molecules at the water–oil interface, and t is the time variable.

The ζ-potential of the cellulose nanoparticles in water was measured by dynamic light scattering (DLS) and electrophoretic mobility using a Zetasizer Nano (ZEN3600 Malvern Instruments Ltd., Malvern, UK) at 25 °C.

Pickering Emulsions Characterization: The microscopic structure of Pickering emulsions prepared with CNCs and CNFs was observed using the optical inverted microscope Nikon Eclipse (TE 2000S, Nikon instruments Europe B.V., Amsterdam, The Netherlands).

The emulsions size distributions were measured via laser diffraction using a Mastersizer 2000 instrument (Malvern instrument Ltd., Malvern, UK), applying the Fraunhofer approximation, which does not require prior knowledge of the optical properties of the sample. The temperature of the cell was maintained at 25 ± 0.5 °C throughout the measurements. Characteristic diameters d(0.1), d(0.5), and d(0.9), representing 10th, 50th (median value), and 90th percentile of the cumulative size distribution of the suspensions, were determined. Additionally, the surface-weighted mean diameter D[3,2] and volume-weighted mean diameter D[4,3] were calculated according to Equations (3) and (4), respectively:

$$D\ [3,2] = \frac{\sum_i n_i d_i^3}{\sum_i n_i d_i^2} \tag{3}$$

$$D\ [4,3] = \frac{\sum_i n_i d_i^4}{\sum_i n_i d_i^3} \tag{4}$$

where n_i is the number of particles of diameter d_i.

The relative span factors were calculated according to Equation (5), to express the distribution width of the droplet size distribution:

$$Span = \frac{d\,(0.9) - d\,(0.1)}{d\,(0.5)} \tag{5}$$

The surface coverage (SC) of NCs of the internal phase of the Pickering emulsions was given by the ratio of the theoretical maximum surface area by the particles (S_P) to the total surface displayed by the oil droplets (S_d), as per Equation (6)[69–71]:

$$SC = \frac{S_P}{S_d} = \frac{m_P \cdot D\,[3,2]}{6 \cdot h \cdot \rho_P \cdot V} \tag{6}$$

where m_P represents the mass of NCs in the Pickering emulsion (g), D[3,2] is the surface-weighted mean diameter, h is the thickness of cellulose fibers (average thickness of CNCs and CNFs fibers is 3.0 ± 0.5 and 10 nm, respectively, as estimated through AFM), ρ_P is the cellulose density (1.6 g cm^{-3}), and V is the volume of oil used in the Pickering emulsion (mL).

The rheological properties of Pickering emulsions were characterized using a rotational rheometer (AR 2000 rheometer, TA instruments, Newcastle, DE, USA), equipped with a concentric cylinder (15 mm stator inner diameter, 28 mm rotor outer diameter, 42 mm cylinder immersed height, 2° cone angle). Viscosity curves were obtained by varying the shear rate from 0.1 s^{-1} up to 200 s^{-1}, with the temperature maintained at 20 °C.

The stability of the emulsions was determined using the turbidimetric method.[72] Absorbance values of freshly prepared emulsions (t_0) and after 30 min (t_{30}) were recorded at 500 nm against a blank (dilution solution), following the introduction of 50 µL of emulsion into 5 mL of 0.1 wt% sodium dodecyl sulfate (SDS) solution. Turbidity (T) was calculated using Equation 7:

$$T = 2.303 \cdot \frac{A \cdot DF}{OP} \tag{7}$$

where A is the absorbance of the sample at t_0 and 500 nm, DF is the dilution factor, and OP is the optical path (1 cm, in the used equipment).

The emulsifying activity index (EAI) and the emulsion stability index (ESI) were calculated using Equations (8) and (9), respectively.

$$EAI\ \left(\frac{m^2}{g}\right) = 2 \cdot \frac{T}{(1-\vartheta) \cdot C \cdot 1000} \tag{8}$$

$$ESI\ (-) = \frac{EAI_{t_0}}{EAI_{t_0} - EAI_{t_{30}}} \cdot 100 \tag{9}$$

where T is the turbidity, ϑ is the volume fraction of oil in the emulsion, and C (g mL^{-1}) is the initial concentration of NCs. EAI_{t0} and EAI_{t30} are the emulsifying activity indexes calculated at 0 and 30 min, respectively.

Statistical Analysis: The experiments were conducted in triplicates, and the resulting values are presented as mean ± standard deviation. Statistical analysis was performed to identify significant differences, with a significance level set at $p < 0.05$. The analysis was carried out using the SPSS 20 statistical package (SPSS Inc., Chicago, IL, USA). The one-way analysis of variance (ANOVA) was employed to assess overall differences among groups, followed by Tukey's test for post-hoc analysis. It is noteworthy that the data exhibited a normal distribution, validating the appropriateness of the selected statistical tests.

Acknowledgements

This study received funding from the MIUR under the project PRIN PANACEA (2017LEPH3M); CUP D44I17000230006.

Open Access Funding provided by Ministero dell'Istruzione, dell'Universitá e della Ricerca within the CRUI-CARE Agreement.

Conflict of Interest

The authors declare no conflict of interest.

Data Availability Statement

The data that support the findings of this study are available from the corresponding author upon reasonable request.

Keywords

emulsifying property, emulsion stability, high-pressure homogenization, nanocellulose, TEMPO oxidation

Received: December 20, 2023
Revised: February 5, 2024
Published online: March 3, 2024

[1] H. Xiong, X. Xie, Y. Li, L. Li, *Colloids Surfaces A Physicochem. Eng. Asp.* **2023**, *673*, 131797.
[2] B. Ding, S. H. Ahmadi, P. Babak, S. L. Bryant, A. Kantzas, *Langmuir* **2023**, *39*, 6975.

[3] J. Wu, G.-H. Ma, *Small* **2016**, *12*, 4633.
[4] Z. Li, D. Yu, *Int. J. Biol. Macromol.* **2023**, *242*, 124942.
[5] Y. Li, D. Yu, X. Wang, Q. Wang, Z. Zhang, W. Liu, *Cellulose* **2022**, *29*, 3253.
[6] N. Nimaming, A. Sadeghpour, B. S. Murray, A. Sarkar, *Trends Food Sci. Technol.* **2023**, *138*, 671.
[7] A. De Bruno, R. Romeo, A. Piscopo, M. Poiana, *J. Sci. Food Agric.* **2020**, *101*, 3535.
[8] S. Zhang, W. Jiang, Z. Zhang, Y. Zhu, L. Wang, J. Fu, *LWT – Food Sci. Technol.* **2020**, *130*, 109369.
[9] Z. Wang, D. Yu, *Cellulose* **2023**, *30*, 9607.
[10] D. Yu, Q. Luo, J. Zhang, Q. Wang, H. Wang, Z. Song, S. Li, W. Liu, F. Zhang, D. Ji, *Cellulose* **2022**, *29*, 8569.
[11] I. Shabir, A. Hussain, K. Kumar, S. Srivastava, V. Kumar, S. Manzoor, S. Manzoor, I. Bashir, *J. Agric. Food Res.* **2023**, *14*, 100853.
[12] Y. Yang, Z. Fang, X. Chen, W. Zhang, Y. Xie, Y. Chen, Z. Liu, W. Yuan, *Front Pharmacol.* **2017**, *8*, 287.
[13] K. J. M. Bishop, C. E. Wilmer, S. Soh, B. A. Grzybowski, *Small* **2009**, *5*, 1600.
[14] H. M. Kipen, D. L. Laskin, *Am. J. Physiol. Lung Cell Mol. Physiol.* **2005**, *289*, L696.
[15] H. Dupont, V. Maingret, V. Schmitt, V. Héroguez, *Macromolecules* **2021**, *54*, 4945.
[16] Y. Xue, Z. Mou, H. Xiao, *Nanoscale* **2017**, *9*, 14758.
[17] S. Meschini, E. Pellegrini, C. A. Maestri, M. Condello, P. Bettotti, G. Condello, M. Scarpa, *J. Biomed. Mater. Res.* **2020**, *108*, 687.
[18] K. J. De France, T. Hoare, E. D. Cranston, *Chem. Mater.* **2017**, *29*, 4609.
[19] C. Jiménez Saelices, I. Capron, *Biomacromolecules* **2018**, *19*, 460.
[20] Y. Habibi, *Chem. Soc. Rev.* **2014**, *43*, 1519.
[21] C. A. Maestri, M. Abrami, S. Hazan, E. Chistè, Y. Golan, J. Rohrer, A. Bernkop-Schnürch, M. Grassi, M. Scarpa, P. Bettotti, *Sci. Rep.* **2017**, *7*, 11129.
[22] H. Voisin, X. Falourd, C. Rivard, I. Capron, *JCIS Open* **2021**, *3*, 100014.
[23] A. Pirozzi, E. Rincón, E. Espinosa, F. Donsì, L. Serrano, *Gels* **2023**, *9*, 958.
[24] W. Qu, Z. Wang, M. Qin, X. Yang, F. Zhang, Z. Wang, D. Ji, D. Yu, *Sep. Purif. Technol.* **2023**, *325*, 124673.
[25] F. Jiang, Y. Lo Hsieh, *ACS Sustainable Chem. Eng.* **2016**, *4*, 1041.
[26] S. H. Teo, C. Y. Chee, M. Z. Fahmi, S. C. W. Sakti, H. V. Lee, *Molecules* **2022**, *27*, 7170.
[27] B. Medronho, B. Lindman, *Curr. Opin. Colloid Interface Sci.* **2014**, *19*, 32.
[28] A. Pirozzi, A. Posocco, F. Donsì, *Food Hydrocoll* **2023**, *145*, 109152.
[29] H. Kargarzadeh, M. Ioelovich, I. Ahmad, S. Thomas, A. Dufresne, in Handb. Nanocellulose Cellul. Nanocomposites, **2017**.
[30] A. Isogai, T. Saito, H. Fukuzumi, *Nanoscale* **2011**, *3*, 71.
[31] T. Thi Thanh Hop, D. Thi Mai, T. Duc Cong, T. T. Y. Nhi, V. Duc Loi, N. Thi Mai Huong, N. Trinh Tung, *Results Chem.* **2022**, *4*, 100540.
[32] H. Xu, J. L. Sanchez-Salvador, A. Blanco, A. Balea, C. Negro, *Carbohydr. Polym.* **2023**, *319*, 121168.
[33] H. Xu, J. L. Sanchez-Salvador, A. Balea, A. Blanco, C. Negro, *Cellulose* **2022**, *29*, 6611.
[34] M. Rajinipriya, M. Nagalakshmaiah, M. Robert, S. Elkoun, *ACS Sustainable Chem. Eng.* **2018**, *6*, 2807.
[35] T. Benselfelt, N. Kummer, M. Nordenström, A. B. Fall, G. Nyström, L. Wågberg, *ChemSusChem* **2023**, *16*, 1.
[36] A. Shinsho, T. Brenner, F. B. Descallar, Y. Tashiro, N. Ando, Y. Zhou, H. Ogawa, S. Matsukawa, *Food Hydrocoll* **2020**, *109*, 105997.
[37] S. Fujisawa, R. Tanaka, Y. Hayashi, Y. Yabuhara, M. Kume, T. Saito, *Polym. J.* **2023**, *55*, 223.
[38] F. Ravera, K. Dziza, E. Santini, L. Cristofolini, L. Liggieri, *Adv. Colloid Interface Sci.* **2021**, *288*, 102344.
[39] Y. Ni, J. Li, L. Fan, *Int. J. Biol. Macromol.* **2020**, *149*, 617.
[40] Y. Goi, S. Fujisawa, T. Saito, K. Yamane, K. Kuroda, A. Isogai, *Langmuir* **2019**, *35*, 10920.
[41] S. Parajuli, E. E. Ureña-Benavides, *Adv. Colloid Interface Sci.* **2022**, *299*, 102530.
[42] A. Pirozzi, R. Capuano, R. Avolio, G. Gentile, G. Ferrari, F. Donsì, *Foods* **2021**, *10*, 1886.
[43] E. J. Foster, R. J. Moon, U. P. Agarwal, M. J. Bortner, J. Bras, S. Camarero-Espinosa, K. J. Chan, M. J. D. Clift, E. D. Cranston, S. J. Eichhorn, D. M. Fox, W. Y. Hamad, L. Heux, B. Jean, M. Korey, W. Nieh, K. J. Ong, M. S. Reid, S. Renneckar, R. Roberts, J. A. Shatkin, J. Simonsen, K. Stinson-Bagby, N. Wanasekara, J. Youngblood, *Chem. Soc. Rev.* **2018**, *47*, 2609.
[44] R. J. Hunter, *Acad. Press* **2013**.
[45] T. Rosén, H. R. He, R. Wang, C. Zhan, S. Chodankar, A. Fall, C. Aulin, P. T. Larsson, T. Lindström, B. S. Hsiao, *ACS Nano* **2020**, *14*, 16743.
[46] L. Solhi, V. Guccini, K. Heise, I. Solala, E. Niinivaara, W. Xu, K. Mihhels, M. Kröger, Z. Meng, J. Wohlert, H. Tao, E. D. Cranston, E. Kontturi, *Chem. Rev.* **2023**, *123*, 1925.
[47] S. A. Kedzior, V. A. Gabriel, M. A. Dubé, E. D. Cranston, *Adv. Mater.* **2021**, *33*, https://doi.org/10.1002/adma.202002404.
[48] N. Rehman, H. Ullah, S. Alam, A. K. Jan, S. W. Khan, M. Tariq, *J. Mater. Environ. Sci.* **2017**, *8*, 1161.
[49] W. Liang, F. Deng, Y. Wang, W. Yue, D. Hu, J. Rong, R. Liu, S. Xiong, Y. Hu, *Food Hydrocoll* **2024**, *149*, 109611.
[50] A. Pirozzi, F. Donsì, *Molecules* **2023**, *28*, 5657.
[51] S. Gharehkhani, E. Sadeghinezhad, S. N. Kazi, H. Yarmand, A. Badarudin, M. R. Safaei, M. N. M. Zubir, *Carbohydr. Polym.* **2015**, *115*, 785.
[52] P. Bertsch, P. Fischer, *Adv. Colloid Interface Sci.* **2020**, *276*, 102089.
[53] L. S. Martins, R. G. dos Santos, M. A. S. Spinacé, *Waste Biomass Valorization* **2022**, *13*, 689.
[54] R. Pal, *AIChE J.* **1996**, *42*, 3181.
[55] I. Kalashnikova, H. Bizot, P. Bertoncini, B. Cathala, I. Capron, *Soft Matter* **2013**, *9*, 952.
[56] H. Dong, Q. Ding, Y. Jiang, X. Li, W. Han, *Carbohydr. Polym.* **2021**, *265*, 118101.
[57] T. Tang, *Nonlinear Anal.: Real World Appl.* **2020**, *56*, 103172.
[58] S. Varanasi, L. Henzel, L. Mendoza, R. Prathapan, W. Batchelor, R. Tabor, G. Garnier, *Front Chem.* **2018**, *6*, 409.
[59] H. Yang, Z. Su, X. Meng, X. Zhang, J. F. Kennedy, B. Liu, *Carbohydr. Polym.* **2020**, *247*, 116712.
[60] A. L. R. Costa, A. Gomes, L. B. Cangussu, R. L. Cunha, L. S. de Oliveira, A. S. Franca, *Food Res. Int.* **2022**, *152*, 110930.
[61] M. S. Reid, M. Villalobos, E. D. Cranston, *Nanoscale* **2016**, *8*, 12247.
[62] T. Yuan, J. Zeng, B. Wang, Z. Cheng, K. Chen, *Carbohydr. Polym.* **2021**, *269*, 118339.
[63] X. Bao, X. Yan, G. Zhang, J. Zhao, Z. Zeng, P. Yu, D. Gong, *Lwt* **2022**, *155*, 112948.
[64] Y. Liu, Y. P. Xie, X. Y. Ma, L. N. Liu, Y. J. Ke, *J. Food Meas. Charact.* **2022**, *16*, 410.
[65] L. Bai, S. Lv, W. Xiang, S. Huan, D. J. McClements, O. J. Rojas, *Food Hydrocoll* **2019**, *96*, 699.
[66] J. Ojala, M. Visanko, O. Laitinen, M. Österberg, J. A. Sirviö, H. Liimatainen, *Molecules* **2018**, *23*, 2765.
[67] D. Da, S. Perez, S. Montanari, M. R. Vignon, *Biomacromolecules* **2003**, *4*, 1417.
[68] E. Mauriello, G. Ferrari, F. Donsì, *Colloids Surf., B* **2021**, *197*, 111424.
[69] K. He, X. Zhang, Y. Li, B. Li, S. Liu, *Food Hydrocoll* **2020**, *101*, 105519.
[70] Z. Hu, T. Patten, R. Pelton, E. D. Cranston, *ACS Sustainable Chem. Eng.* **2015**, *3*, 1023.
[71] I. Kalashnikova, H. Bizot, B. Cathala, I. Capron, *Langmuir* **2011**, *27*, 7471.
[72] S. De Maria, G. Ferrari, P. Maresca, *Innov. Food Sci. Emerg. Technol.* **2016**, *33*, 67.

